Helical tractor beam: analytical solution of Rayleigh particle dynamics

Luis Carretero,[1,*] **Pablo Acebal,**[1] **Celia Garcia,**[2] **and Salvador Blaya**[1]

[1]*Universidad Miguel Hernández, Dpto. de Ciencia de Materiales Óptica y Tecnología electrónica, Avda. de la Universidad, 3202, Elche, Alicante, Spain*
[2]*Universidad de Alicante, Dpto. Óptica, Farmacología y Anatomía, Alicante, Spain*

[*]*luis@dite.umh.es*

Abstract: We analyze particle dynamics in an optical force field generated by helical tractor beams obtained by the interference of a cylindrical beam with a topological charge and a co-propagating temporally de-phased plane wave. We show that, for standard experimental conditions, it is possible to obtain analytical solutions for the trajectories of particles in such force field by using of some approximations. These solutions show that, in contrast to other tractor beams described before, the intensity becomes a key parameter for the control of particle trajectories. Therefore, by tuning the intensity value the particle can describe helical trajectories upstream and downstream, a circular trajectory in a fixed plane, or a linear displacement in the propagation direction. The approximated analytical solutions show good agreement to the corresponding numerical solutions of the exact dynamical differential equations.

© 2015 Optical Society of America

OCIS codes: (260.2110) Electromagnetic optics; (260.5430) Polarization; (140.7010) Laser trapping; (350.4855) Optical tweezers or optical manipulation.

References and links

1. A. Ashkin, "Acceleration and trapping of particles by radiation presure," Phys. Rev. Lett. **24**, 156–159 (1970).
2. T. Cizmar, V. Garces-Chavez, K. Dholakia, and P. Zemanek, "Optical conveyor belt for delivery submicron objects," Appl. Phys. Lett. **86**, 174101 (2005).
3. T. Cizmar, M. Siler, and P. Zemanek, "An optical nanotrap array movable over a milimetre range," Appl. Phys. B **84**, 197–203 (2006).
4. S.-H. Lee, Y. Roichman, and D. G. Grier, "Optical solenoid beams," Opt. Express **18**(7), 6988–6993 (2010).
5. D. B. Ruffner and D. G. Grier, "Optical conveyors: A class of active tractor beams," Phys. Rev. Lett. **109**, 163903 (2012).
6. O. Brzobohaty, V. Karasek, M. Sailer, L. Chavatal, T. Cizmar, and P. Zemanek, "Experimental demonstration of optical transport sorting and sef-arrangement using a tractor beam," Nat. Photonics **7**, 123–127 (2013).
7. V. Shvedov, A. R. Davoyan, C. Hnatovsky, N. Engheta, and W. Krolikowski, "A long-range polarization-controlled optical tractor beam," Nat. Photonics **8**(11), 846–850 (2014).
8. Huajin Chen, Shinyang Liu, Jiang Zi, and Zhifang Lin, "Fano resonance-induced negative optical scattering force on plasmonic nanoparticles," ACS Nano **9**(2), 1926–1935 (2015).
9. S. Sukhov and A. Dogariu, "Negative nonconservative forces: optical 'tractor beams' for arbitrary objects," Phys. Rev. Lett. **107**, 203602 (2011). URL http://link.aps.org/doi/10.1103/PhysRevLett.107.203602.
10. L. Carretero, P. Acebal, and S. Blaya, "Three-dimensional analysis of optical forces generated by an active tractor beam using radial polarization," Opt. Express **22**, 3284–3295 (2014).
11. J. Durnin, "Exact solutions for nondiffracting beams. I. The scalar theory," J. Opt. Soc. Am. A **4**(4), 651–654 (1987).
12. H. Chen, N. Wang, W. Lu, S. Liu, and Z. Lin, "Tailoring azimuthal optical force on lossy chiral particles in Bessel beams," Phys. Rev. A **90**, 043850 (2014). URL http://link.aps.org/doi/10.1103/PhysRevA.90.043850.

13. L. Carretero, P. Acebal, C. Garcia, and S. Blaya, "Periodic trajectories obtained with an active tractor beam using azimuthal polarization: design of particle exchanger," IEEE Photon. J. **7**(1), 1–12 (2015).
14. C. Vetter, T. Eichelkraut, M. Ornigotti, and A. Szameit, "Generalized radially self-accelerating helicon beams," Phys. Rev. Lett. **113**, 183901 (2014).
15. P. C. Chaumet and M. Nieto-Vesperinas, "Time-averaged total force on a dipolar sphere in an electromagentic fiel," Opt. Lett. **25**, 1065–1067 (2000).
16. M. Nieto-Vesperinas, J. S??enz, R. Gomez-Medina, and L. Chantada, "Optical forces on small magnetodielectric particles," Opt. Express **18**, 11428–11443 (2010).
17. N. Wang, J. Chen, S. Liu, and Z. Lin, "Dynamical and phase-diagram study on stable optical pulling force in Bessel beams," Phys. Rev. A **87**, 063812 (2013).

1. Introduction

Optical trapping of particles [1] has become an essential tool for the manipulation of small objects in many disciplines such as physics or biology. In this way, new advances in laser beam control have led to the experimental realization of tractor beams that can draw particles toward light sources [2–7]. Recently, it was pointed out that Fano resonance of a composite metallic nanoparticle can induce a negative pulling force [8]. Unlike conventional optical tweezers, which rely on adjusting the positions of intensity gradients to move objects, tractor beams can exert non-conservative pulling forces on particles by continuously dragging them towards the beam sources [9]. In these tractor beams, the dynamics of particles has also been analyzed; in particular, our team has theoretically studied the case of radially polarized zero-order Bessel tractors beam [10], analyzing the trajectories that, in general, are linear [2, 3], [5]. As found from many theoretical and experimental studies, non-diffracting beams are promising candidates for realizing tractor beams due to their unique properties of maintaining both intensity and spatial extent in the direction of propagation [11]. Thus, a great variety of optical fields, ranging from the fundamental Gaussian beam, Laguerre-Gaussian beam, Airy beam, and Bessel beam (BB) to the plasmon-based optical field, has been employed to achieve optical micromanipulations [12] . In this sense, more complex trajectories can be obtained using, for example, azimuthally polarized beams [13]. Moreover, recently, an interesting class of beam that could be used for sorting, mixing, or cell extraction applications could be obtained using generalized radially self-accelerating helicon beams [14] due to the three-dimensional spiraling trajectories that could be generated. In fact, a similar procedure was used in [4] for obtaining solenoidal waves through a particular superposition of many m-th order Bessel beams that do not differ in their relative temporal phase. In relation to these points, in this paper we propose to generate a helical tractor beam by means of the interference of a plane wave and a cylindrical beam (that differ in their relative temporal phase) and it is a paraxial solution to the Helmholtz equation. For this, we are going to analytically and numerically analyze the dynamics of Rayleigh particles inside this tractor beam.

2. Theoretical background

We consider a linearly polarized electric field $\vec{E}$, obtained by a superposition of a plane wave (PW) and a paraxial solution of the Helmholtz equation in (r,ψ,z) cylindrical coordinates (i.e., a cylindrical beam (CB) like Bessel beams or Laguerre-Gaussian beams, etc.) propagating in the $\hat{z}$ direction given by:

$$\vec{E} = A\left[\eta\, Exp(i(k_1 z - \xi t)) + Exp(i(k_2 z + m\,\psi))G(r)\right]\hat{x} \tag{1}$$

where k_1 and k_2 are the wave numbers of the beams in a medium of refractive index n, $G(r)$ is the radial solution to the Helmholtz equation in cylindrical coordinates, A is the electric field amplitude, $0 < \eta < 1$ is the beam ratio between the plane wave and CB beam. The PW and the

CB beams differ in their relative phases not only in the helical phase given by the topological charge m, but also in a temporal linear function ξt that is critical for tractor working [5]. It should be noted, that the solenoidal beam described by Eq.(1) operates due to the relative phase difference between the PW and CB beams (ξt), and it is quite different to that showed in [4], because the second one uses periodic axial intensity gradients with discrete propagation invariance to achieve forward scattering from the interference between the incident field and the dipole radiation field of an illuminated object [5].

The optical forces acting on a particle in the Rayleigh regime (particle radius $r_p << \lambda$) as a consequence of an electric field given by Eq. (1) can be expressed according to [15], as:

$$\vec{F} = \frac{1}{2}\Re\left[\hat{\alpha}E_x\left(\frac{\partial E_x^*}{\partial r}\hat{r} + \frac{1}{r}\frac{\partial E_x^*}{\partial \psi}\hat{\psi} + \frac{\partial E_x^*}{\partial z}\hat{z}\right)\right] \tag{2}$$

where $\Re$ denotes the real part of the expression, * is the complex conjugate value, and $\hat{\alpha}$ is the complex polarizability of the particle:

$$\hat{\alpha} = \alpha_R + i\alpha_I \tag{3}$$

α_R and α_I are the real and imaginary parts of the polarizability, respectively, which for the dielectric particles can be obtained, for example, from [16].

The deterministic trajectories of particles can be obtained by solving the equation:

$$m_0\frac{d^2\vec{R}}{dt^2} = \vec{F}(\vec{R}(t)) - \kappa\frac{d\vec{R}}{dt} \tag{4}$$

where $\vec{R}(t)$ is the position vector of the particle at time t, m_0 is the particle mass, and $-\kappa\frac{d\vec{R}}{dt}$ is the frictional force. It is important to remark that Eq. (4) does not take into account the thermal effects, that could be included by using the Langevin equation instead [10].

2.1. Approximated solution

Assuming that the inertia force is smaller than the drag force (over-damped case), the left-hand side of Eq.(4) vanishes, so introducing Eqs.(1,2) and 3 in Eq. (4), motion particle equations can be written as:

$$\begin{bmatrix} \dot{r} \\ \dot{\psi} \\ \dot{z} \end{bmatrix} = \mathbf{M}\begin{bmatrix} 1 \\ Sin[H(t)] \\ Cos[H(t)] \end{bmatrix} \tag{5}$$

where $\dot{p}$, $(p = r, \psi, z)$ represents the temporal derivative of the p-coordinate, the function $H(t) = (k_1 - k_2)z(t) - \xi t - m\psi(t) = \Delta_k z(t) - \xi t - m\psi(t)$ describes the temporal coupling of the axial and azimuthal variables, and the constant matrix $\mathbf{M}$ is defined as:

$$\mathbf{M} = \Omega\begin{bmatrix} \alpha_R G(r)\dot{G}(r) & -\alpha_I\eta\dot{G}(r) & \alpha_R\eta\dot{G}(r) \\ \frac{m\alpha_I G(r)^2}{r^2} & \frac{m\alpha_R\eta G(r)}{r^2} & \frac{m\alpha_I\eta G(r)}{r^2} \\ \alpha_I(k_1\eta^2 + k_2 G(r)^2) & (k_2 - k_1)\alpha_R\eta G(r) & (k_1 + k_2)\alpha_I\eta G(r) \end{bmatrix} \tag{6}$$

where we have used the parameter $\Omega = A^2/(2\kappa) = I_0/(\kappa n c\varepsilon_0)$ (I_0 being the intensity of the field $I_0 = nc\varepsilon_0 A^2/2$). The motion equation for the radial coordinate is a typical equation for an optical trap, where the particles are quickly trapped in the radial positions r_q that satisfy, independently of their axial and azimuthal positions, the equation $\dot{G}(r)|_{r=r_q} = 0$.

Therefore, at these points r_q, matrix elements M_{11}, M_{12} and M_{13} are null, so Eq. (5) can be

rewritten as:

$$\dot{r} = 0 \Rightarrow r = r_q \tag{7}$$

$$\dot{\psi} = v_{\psi 0} + v_{\psi} Cos(H(t) - \alpha_{\psi}) \tag{8}$$

$$\dot{z} = v_{z0} + v_z Cos(H(t) - \alpha_z) \tag{9}$$

where we have introduced the parameters:

$$v_{z0} = \Omega \, \alpha_I \, (k_1 \, \eta^2 + k_2 \, G(r_q)^2)$$

$$v_{\psi 0} = \frac{\Omega \, m \, \alpha_I \, G(r_q)^2}{r_q^2}$$

$$v_z = \Omega \, \eta \, |G(r_q)| \sqrt{(k_1 + k_2)^2 \, \alpha_I^2 + (k_1 - k_2)^2 \, \alpha_R^2} \tag{10}$$

$$Tan(\alpha_z) = \frac{(k_2 - k_1) \alpha_R}{(k_2 + k_1) \alpha_I}$$

$$v_{\psi} = \frac{\Omega \, \eta \, |m \, G(r_q)| \sqrt{\alpha_I^2 + \alpha_R^2}}{r_q^2}$$

$$Tan(\alpha_{\psi}) = \frac{\alpha_R}{\alpha_I}$$

Parameters v_{z0} and $v_{\psi 0}$ represent the axial and angular velocity that the particles would obtain in absence of interference, namely, if the electric fields in Eq.(1) were incoherent, while v_z and v_{ψ} correspond to the axial and angular velocity due to the interference, respectively.
In order to solve the general case given by Eqs.(8,9), it is necessary to uncouple the $\psi(t)$ and $z(t)$ variables. To do this, removing function H(t) from Eqs.(8,9) obtains that axial velocity $\dot{z}$ and angular velocity $\dot{\psi}$ fulfill the following ellipse equation:

$$\left(\frac{\dot{z} - v_{z0}}{v_z} \right)^2 + \left(\frac{\dot{\psi} - v_{\psi 0}}{v_{\psi}} \right)^2 - 2 \left(\frac{\dot{z} - v_{z0}}{v_z} \right) \left(\frac{\dot{\psi} - v_{\psi 0}}{v_{\psi}} \right) Cos(\delta) = Sin(\delta)^2 \tag{11}$$

where $\delta = \alpha_z - \alpha_{\psi}$. Using the definitions of α_z and α_{ψ} given in Eq. (10), the key parameters $Cos(\delta)$ and $Sin(\delta) = [1 - Cos(\delta)^2]^{1/2}$ can be written as:

$$Cos(\delta) = \frac{(k_1 + k_2)\alpha_I^2 + (-k1 + k2)\alpha_R^2}{(k1 + k2)\alpha_I \sqrt{(\alpha_I^2 + \alpha_R^2)(1 + \frac{(k1 - k2)^2 \alpha_R^2}{(k1 + k2)^2 \alpha_I^2})}}$$

We center our study on the case of Rayleigh dielectric particles so we can assume that $\alpha_R >> \alpha_I$ [3] and then, using Eq. (12), we can approximate:

$$Cos(\delta) \approx -Sign(k_1 - k_2) = -1 \tag{12}$$

$$Sin(\delta) \approx -\frac{2k_1 \alpha_I}{\alpha_R |k_1 - k_2|} < 0 \tag{13}$$

where we have assumed that the wave number of PW is higher than the one of CB ($k_1 > k_2$). For Rayleigh particles, $|Sin(\delta)| << 1$. Therefore, Eq.(11) can be simplified to:

$$\left(\frac{\dot{z} - v_{z0}}{v_z} + \frac{\dot{\psi} - v_{\psi 0}}{v_{\psi}} \right) = |Sin(\delta)| \tag{14}$$

Thus, by solving differential equation 14, the temporal relation between axial and azimuthal coordinates is given by:

$$\psi(t) = A_1 t + A_2 z(t) + A_3 \qquad (15)$$

where:

$$A_1 = v_{\psi 0} + v_\psi \left(\frac{v_{z0}}{v_z} + |Sin(\delta)| \right) \qquad (16)$$

$$A_2 = \frac{-v_\psi}{v_z} \qquad (17)$$

$$A_3 = \psi_0 - A_2 z_0 \qquad (18)$$

with ψ_0 and z_0 the initial position coordinates of the particle.

Therefore, by using the temporal relation between the axial and azimuthal coordinates (Eq. (15)), it is possible to express $H(t)$ only as a function of the time and the $z(t)$ or $\psi(t)$ coordinate, so differential equations 8-9 can be written as:

$$\dot{z} = v_{z0} + v_z Cos\left[(\Delta_k - mA_2) z(t) - (\xi + mA_1)t - mA_3 - \alpha_z \right]$$
$$\dot{\psi} = v_{\psi 0} + v_\psi Cos\left[\left(\frac{\Delta_k}{A_2} - m \right) \psi(t) - \left(\xi + \frac{\Delta_k A_1}{A_2} \right) t - \frac{\Delta_k A_3}{A_2} - \alpha_\psi \right] \qquad (19)$$

Previous equations show that trapped particles are axially and azimuthally translated with tractor velocities:

$$v_{zt} = \frac{(\xi + mA_1)}{\Delta_k - mA_2} \qquad (20)$$

$$v_{\psi t} = \frac{(\xi A_2 + \Delta_k A_1)}{\Delta_k - mA_2} \qquad (21)$$

Analytical solutions to Eqs.(19) are given by:

$$z(t) = v_{zt} t + f_z(t)$$
$$\psi(t) = v_{\psi t} t + f_\psi(t) \qquad (22)$$

where f_z and f_ψ are the functions:

$$f_z(t) = \frac{mA_3 + \alpha_z + 2Tan\left[\frac{\sqrt{v_z + v_{z0} - v_{zt}}\, Tanh[\frac{\Delta_k - mA_2}{2} \sqrt{v_z + v_{z0} - v_{zt}} \sqrt{v_z - v_{z0} + v_{zt}}(t - c1)]}{\sqrt{v_z - v_{z0} + v_{zt}}} \right]^{-1}}{\Delta_k - mA_2} \qquad (23)$$

$$f_\psi(t) = \frac{\Delta_k A_3 + \alpha_\psi A_2 + 2A_2 Tan\left[\frac{\sqrt{v_\psi + v_{\psi 0} - v_{\psi t}}\, Tanh[\frac{\Delta_k - mA_2}{2A_2} \sqrt{v_\psi + v_{\psi 0} - v_{\psi t}} \sqrt{v_\psi - v_{\psi 0} + v_{\psi t}}(t - c2)]}{\sqrt{v_\psi - v_{\psi 0} + v_{\psi t}}} \right]^{-1}}{\Delta_k - mA_2}$$
$$(24)$$

c_1 and c_2 are constants that take boundary conditions into account. Moreover, it must be noted that f_z and f_ψ are bounded functions that verify $f_z < v_{zt} t$ and $f_\psi < v_{\psi t} t$, so Eqs.(22) can be approximated to:

$$z(t) \approx v_{zt} t$$
$$\psi(t) \approx v_{\psi t} t \qquad (25)$$

As a consequence, the position's particle vector $\vec{R}(t)$ can be written as:

$$\vec{R}(t) = r_q \, Cos(v_{\psi t} t)\hat{x} + r_q \, Sin(v_{\psi t} t)\hat{y} + p\frac{v_{\psi t}}{2\pi}t\hat{z} \qquad (26)$$

where $p = \frac{2\pi v_{zt}}{v_{\psi t}}$. Equation 26 shows that particles describe a helical motion where $\hat{z}$ is the axis of the helix, r_q is the radius, p is the pitch and $v_{\psi t}$ is the angular frequency of the particle vector. Then, $\vec{R}(t)$ traces a helix whose end point moves around a cylinder once every $\frac{2\pi}{v_{\psi t}}$ units of time and moves a distance p in the direction $\hat{z}$ for every revolution around the cylinder.

2.2. Tractor velocity intensity dependence

In this section, we are going to assume that $m \geq 0$. Parameters A_1 and A_2 play an important role in the movement of particles, so it is important to analyze their relative values. Taking into account the definitions given by Eqs.(10), it can be deduced that velocities $v_{\psi 0}, v_\psi, v_{z0}, v_z$ are greater than or equal to zero, and as a result, $A_1 \geq 0$ and $A_2 \leq 0$. It is important to remark that the A_1 parameter depends on the position of the maximum r_q where the particle is located, and due to the dependence of velocities $v_{\psi 0}$ and v_ψ on Ω, A_1 is proportional to the intensity. However, A_2 depends only on r_q, while it does not on I_0. According to this, we can write $A_1 = a_1(r_q)I_0$ and $A_2 = a_2(r_q)$, with $(a_1(r_q) \geq 0$ and $a_2(r_q) \leq 0)$. Taking into account this fact, the tractor velocities and pitch can be rewritten as:

$$\begin{aligned} v_{zt} &= \frac{(\xi + m\,a_1(r_q)I_0)}{\Delta_k - m\,a_2(r_q)} \\ v_{\psi t} &= \frac{(\xi\,a_2(r_q) + \Delta_k\,a_1(r_q)I_0)}{\Delta_k - m\,a_2(r_q)} \\ p &= \frac{2\pi(\xi + m\,a_1(r_q)I_0)}{(\xi\,a_2(r_q) + \Delta_k\,a_1(r_q)I_0)} \end{aligned} \qquad (27)$$

Previous equations show that pitch, axial, and azimuthal tractor velocities (and as a consequence trajectories given in Eq.(26)) depend on the intensity, the topological charge, the local maximum where the particle is located, the relative phase difference between the PW and CB beam, and of course, the amplitude ratio η between the beams. It can be noted that in the limit case in which $\eta = 0$, there is no action of the tractor beam ($\xi = 0$) and the particle dynamic is controlled only by the Bessel beam. The stability of the negative pulling force for a particle in a Bessel beam has been discussed in the reference [17]. In the other cases, the influence of amplitude ratio η in the particle movement is included in the a_1 parameter in a complex way. In this sense, a_1 shows a parabolic dependence on η, but the parabola's coefficients change basically with radial position, topological charge, and intensity.

If there is no topological charge ($m = 0$), then v_ψ and $v_{\psi 0}$ are null, as a consequence $a_1(r_q) = a_2(r_q) = 0$, and then from Eq.(27), it can be deduced that azimuthally tractor velocity $v_{\psi t}$ is zero and the axial tractor velocity is equal to that obtained in reference [5] ($v_{zt} = \frac{\xi}{\Delta_k}$). In this case, all particles are translated upstream or downstream (depending on the sign of the ξ parameter), and the helix trajectory given by Eq. (26) is reduced to a linear movement in the $\hat{z}$ direction [5]. Therefore, the lack of topological charge implies that axial tractor velocity does not depend on intensity I_0.

In the case of null relative phase difference $\xi = 0$ and non-null topological charge $m \neq 0$, it can be also deduced from Eqs.(27,26) that a helical trajectory is obtained with the tractor velocities

and pitch:

$$v_{zt} = \frac{m\,a_1(r_q)I_0}{\Delta_k - m\,a_2(r_q)}$$

$$v_{\psi t} = \frac{\Delta_k\,a_1(r_q)I_0}{\Delta_k - m\,a_2(r_q)} \qquad (28)$$

$$p = \frac{2\pi m}{\Delta_k}$$

where, under these conditions, $v_{zt} > 0$; then, particles move upstream describing a helix in the positive $\hat{z}$ direction with velocities that are proportional to the intensity I_0 and vary for every r_q position. It is interesting to point out that particles can not be moved downstream for any m parameter value. Furthermore, in this case, the pitch is constant and independent of the intensity and the radial position of particles r_q.

The most interesting cases are obtained when the relative phase difference ξ and the topological charge m are both non-null. Eqs. (27) show that v_{zt} can be positive, negative, or null, and $v_{\psi t}$ is ever positive or null depending on the intensity I_0 and the position of the intensity maximum r_q. Thus, the behavior of particle movement could be very different by adequately choosing the intensity and ξ ratio, so we can obtain:

1. All trapped particles describe a helix upstream.
   In this case, it is necessary that $v_{zt} > 0$, so, according to Eq.(20):

   $$v_{zt} > 0 \iff \xi + m\,a_1(r_q)I_0 > 0 \qquad (29)$$

   If ξ is positive, independently of the position trap r_q, this inequality is verified for all particles. For negative values of the ξ parameter, this inequality is fulfilled for particles located at position traps r_q that satisfy the condition $|\xi| < m\,a_1(r_q)I_0$, so negative values of ξ can generate upstream movement in the helical tractor beams.

2. All trapped particles describe a helix downstream.
   In this case, it is necessary that $v_{zt} < 0$, so, according to Eq.(20):

   $$v_{zt} < 0 \iff m\,a_1(r_q)I_0 < -\xi \qquad (30)$$

   This inequality is verified only if ξ is negative and $|\xi| > m\,a_1(r_q)I_0$.

3. All trapped particles describe a helix except the corresponding ones located at the intensity maxima position $r_q = r_{q\psi}$ that describe a circular movement at the initial z_0 plane.
   In this case, it is necessary that $v_{zt}(r_{q\psi}) = 0$, so, according to Eq.(20):

   $$v_{zt} = 0 \iff I_0 = I_{q\psi} = \frac{-\xi}{m\,a_1(r_{q\psi})} \qquad (31)$$

   Then, intensity $I_{q\psi}$ selects particles located at the radial trap $r_{q\psi}$ and moves them in a circular trajectory at the initial z_0 plane, while all the other ones describe helical trajectories. Then, it is possible to control the type of particle' movement by using the adequate intensity. Note that the intensity $I_{q\psi}$ is positive only if ξ is negative, so, in general, in this case, the helical movement will be downstream.

4. All trapped particles describe a helix upstream except the ones located at intensity maxima position $r_q = r_{qz}$ that show a linear movement in the $\hat{z}$ direction.

In this case, it is necessary that $v_{zt} > 0$ for all particles (so according to the discussion of point 1, we choose $\xi > 0$) and $v_{\psi t}(r_{qz}) = 0$, so, from Eq.(20):

$$v_{\psi t} = 0 \iff I_0 = I_{qz} = \frac{-\xi\, a_2(r_{qz})}{\Delta_k\, a_1(r_{qz})} \tag{32}$$

Then, intensity I_{qz} selects particles located at the radial trap r_{qz} and moves them linearly in the $\hat{z}$ direction, while all the other ones, describe upstream helical trajectories. Then, by using the right intensity, linear movement along the $\hat{z}$ direction and an upstream helix can be chosen. Note that the intensity I_{qz} is positive only when ξ is positive, so it is not possible to obtain a downstream helix movement.

3. Comparison between exact numerical results and approximations

In this section, we are going to compare our approximated solutions described in previous sections and the corresponding exact numerical solution to Eq.(4). For solving coupled differential equations we have used a Runge-Kutta fourth-order method using the same boundary conditions in numerical calculations as in approximated solutions (with initial velocity particles equal to 0). We have also used a Bessel beam as the CB beam in Eq.(1), then we take $k_2 = k_1 Cos(\theta)$ and the radial function $G(r) = J_m(k_1 Sin(\theta)r)$, with J_m the Bessel function of the first kind of order m. Moreover, the constants $\kappa = 6\pi\eta_1 r_p$ and $m_0 = \frac{4}{3}\rho\pi r_p^3$ (with r_p the particle radius) have been obtained using the water viscosity coefficient $\eta_1 = 8.9 \times 10^{-4}$ (Pa s) and the material density (PMMA) $\rho = 1.19 \times 10^3$ (Kg m^{-3}).The other numerical values used in our study are given in table 1.

Table 1. Values of the parameters used in the numerical simulations

θ	λ (nm)	ξ (Hz)	r_p	n= $\sqrt{\varepsilon}$	ε_p	η
$\frac{3\pi}{23}$	633	± 10	$\frac{\lambda}{30}$	1.33	2.223	0.5

Due to the large number of possible cases, we will focus on the results described by Eqs.(31,32).

Figure 1 shows the axial length, axial velocity, angular velocity and pitch obtained at a fixed time $t = 5\,s$ for $\xi = -10\,Hz$ as a function of the intensity position maxima r_q using three different topological charges ($m = 1, 2, 3$) by accomplishing $v_{zt} = 0$ (Eq.(31)) at the first maximum position r_1. Under this condition, the obtained intensities are $I_{1\psi} = 0.71, 0.6, 0.56\,W/cm^2$ for topological charges $m = 1, 2, 3$, respectively. As can be observed, good agreement is obtained between approximated analytical equations and exact numerical results. As was expected, particles located at the r_1 maxima position do not move axially, but describe a circular movement of angular velocity $\dot{\psi} = v_{\psi t} \approx \frac{-\xi}{m}$. It can also be observed that, for a fixed topological charge, axial displacement increases as r_q rises, although when the topological charge increases, axial length is lower for equivalent maxima r_q. 3D helical trajectories can be observed in Fig. 2 for the particular cases of a topological charge $m = 2$ and condition $v_{zt} = 0$ obtained with an intensity $I_0 = I_{1\psi} = 0.6W/cm^2$. It can be seen that particles located at maxima r_2, r_3 and r_4 describe a downstream helix, with the numerical result very close to the obtained one by means of analytical Eqs.(26). As was previously mentioned, the particles located at the maximum r_1 describe a circular trajectory.

Finally, we are going to realize the corresponding study when $v_{\psi t} = 0$ (Eq.(32)). Figure 3 shows the axial length, axial velocity, angular velocity, and pitch obtained at a fixed time $t = 5\,s$ for $\xi = 10\,Hz$ as a function of the intensity position maxima r_q using three different topological
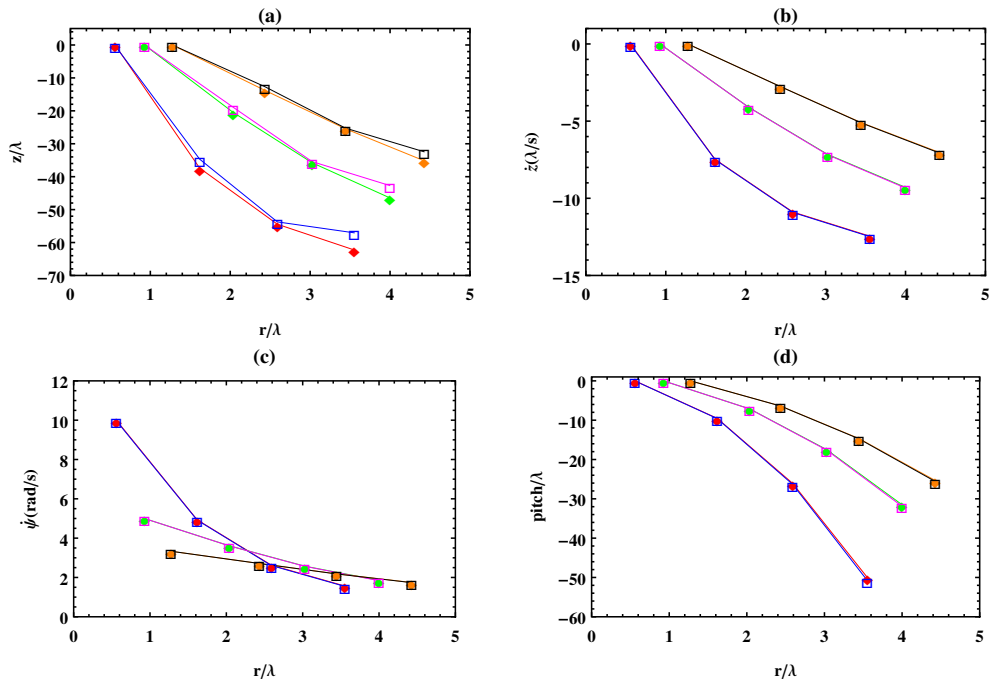
Fig. 1. (a) Axial length, (b) axial velocity, (c) angular velocity, and (d) pitch at a fixed time $t = 5\,s$ and $\xi = -10\,Hz$ as a function of the intensity position maxima r_q. Topological charge $m = 1$: (approximated red, numerical blue); $m = 2$: (approximated green, numerical magenta); $m = 3$: (approximated orange, numerical black).

charges ($m = 1, 2, 3$) with the condition given by Eq.(32) $v_{\psi t} = 0$ for the first maximum position r_1. Under this condition, the intensities are $I_{1z} = 4.9, 6.1, 6.8\,W/cm^2$ for the topological charges $m = 1, 2, 3$ respectively. As can be observed, good agreement between approximated analytical equations and exact numerical results is shown, but small differences can be noted for the topological charge $m = 1$ case. From Fig. 3, as was mentioned, particles located at the
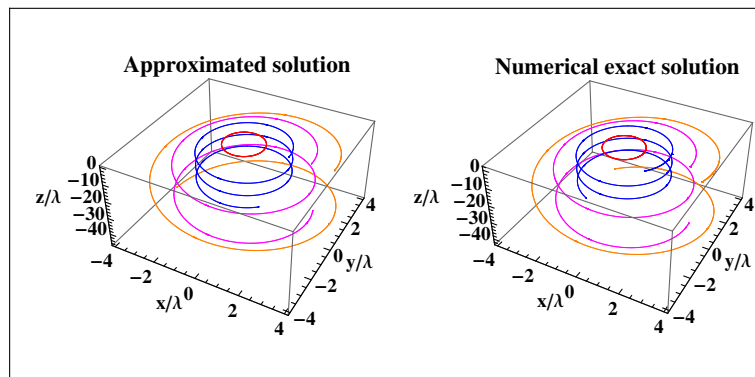

Fig. 2. Numerical and analytical helical trajectories for a topological charge $m = 2$, and condition $v_{zt} = 0$ obtained with an intensity $I_0 = I_{1\psi} = 0.6\,W/cm^2$.
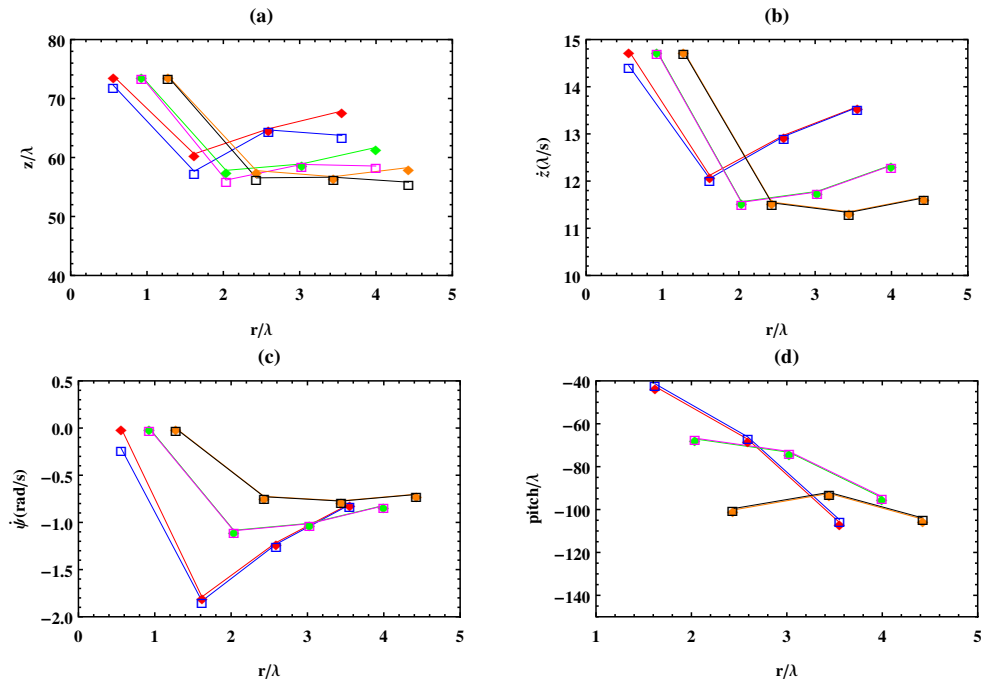
Fig. 3. (a) Axial length, (b) axial velocity, (c) angular velocity, and (d) pitch at a fixed time $t = 5\,s$ and $\xi = 10\,Hz$ as a function of the intensity position maxima r_q. Topological charge $m = 1$: (approximated red, numerical blue); $m = 2$: (approximated green, numerical magenta); $m = 3$: (approximated orange, numerical black).

r_1 maxima describe a linear movement on the z-axis because the angular velocity $\dot{\psi} = v_{\psi t} = 0$. 3D helical trajectories can be observed in Fig. 4 for the particular cases of a topological charge $m = 2$, and the condition $v_{\psi t} = 0$ obtained by an intensity $I_0 = I_{1\psi} = 6.1\,W/cm^2$. It can be seen that particles located at the maxima r_2, r_3, and r_4 describe an upstream helix, with the numerical result very close to that obtained by means of analytical Eqs. (26).
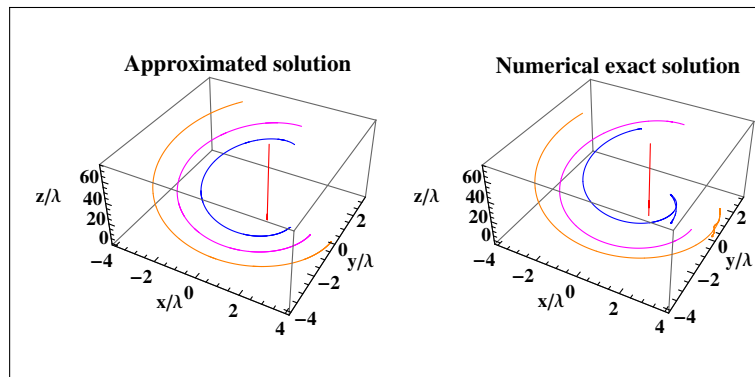

Fig. 4. Numerical and analytical helical trajectories for a topological charge $m = 2$, and condition $v_{\psi t} = 0$ obtained with an intensity $I_0 = I_{1z} = 6.1\,W/cm^2$.

4. Conclusions

Particle dynamic trajectories inside helical tractor beams have been analyzed. We have demonstrated that nanoparticles in helical tractor beams can describe helical upstream, helical downstream, linear, or circular trajectories depending on the tractor velocities (axial and angular), that can be controlled by means the intensity of the beam. This dependence of the intensity of velocities results from the coupling between axial and azimuthal coordinates in the dynamic equations. These results, could be applied in the field of particle sorting and assembly of synthetic or biological nano-objects.